Combining Strings and Necklaces for Interactive Three-Dimensional Segmentation of Spinal Images Using an Integral Deformable Spine Model

Ghebreab, S.; Smeulders, A.W.M.

Publication date
2004

Published in
IEEE Transactions on Biomedical Engineering

Combining Strings and Necklaces for Interactive Three-Dimensional Segmentation of Spinal Images Using an Integral Deformable Spine Model

Sennay Ghebreab* and Arnold W. M. Smeulders, *Senior Member, IEEE*

***Abstract*—Segmentation of the spine directly from three-dimensional (3-D) image data is desirable to accurately capture its morphological properties. We describe a method that allows true 3-D spinal image segmentation using a deformable integral spine model. The method learns the appearance of vertebrae from multiple continuous features recorded along vertebra boundaries in a given training set of images. Important summarizing statistics are encoded into a necklace model on which landmarks are differentiated on their free dimensions. The landmarks are used within a priority segmentation scheme to reduce the complexity of the segmentation problem. Necklace models are coupled by string models. The string models describe in detail the biological variability in the appearance of spinal curvatures from multiple continuous features recorded in the training set. In the segmentation phase, the necklace and string models are used to interactively detect vertebral structures in new image data via elastic deformation reminiscent of a marionette with strings allowing for movement between interrelated structures. Strings constrain the deformation of the spine model within feasible solutions. The driving application in this work is analysis of computed tomography scans of the human lumbar spine. An illustration of the segmentation process shows that the method is promising for segmentation of the spine and for assessment of its morphological properties.**

***Index Terms*—Energy-minimization methods, functional data analysis, interactive image segmentation, landmark-based object segmentation, statistical deformable models.**

I. Introduction

THREE-DIMENSIONAL (3-D) image segmentation is an essential task for image-based analysis of spinal morphology. This is difficult to achieve fully automatically with current segmentation methods due to the articulate visual appearance of the spine and its close contact proximity to ribs and other organs. The shape of vertebrae exhibits many protrusions and topological accidents, violating the smoothness assumption under which many segmentation methods operate. Apart from this, their gray-level appearance is in most cases far from evident due to insufficient image contrast, interfering anatomical structures, and other local irregularities. A segmentation method that does not take into consideration the inhomogeneous shape and gray-level appearance of the spine will encounter serious problems and fail. It is, therefore, desirable to construct a spine segmentation method that exploits shape and gray-level inhomogeneities to facilitate image segmentation rather than being hampered by such inhomogeneities.

Commonly, spinal image segmentation is done by fitting *a priori* geometrical models of vertebrae and *a priori* spatial models of inter-relationships between vertebrae to edges in the image. There are three important shortcomings to this. First, the models only capture *a priori* shape and spatial information, while the appearance of the spine in the image is also defined by gray-level features. There is also a need to model gray-level appearance [1]. Second, geometrical and spatial models often lack expressive power to catch the full range of feasible image appearances of the spine. Third, geometrical and spatial models often offer no room for human-computer interaction, which is still crucial for segmentation. In order to construct an apt spine segmentation model it is natural i) to model shape as well as gray-level features, ii) to address the natural variability of these features and iii) to use human-computer interaction for exploiting inhomogeneities in these features

This paper presents a segmentation method that combines strings [2] and necklaces [3] into a deformable integral spine model. Strings focus on learning the most relevant biological variation in the visual appearance of the spine as a whole under the premise that this variation can be well captured in a statistical sense. Learning in this context is reduced to statistical analysis of multiple continuous shape and gray level features in a given training set of segmented spinal images. Necklaces aim to exploit inhomogeneities in multiple continuous shape and gray-level features of vertebrae that are also deduced from a given training set of segmented spinal images. The premise is that feature inhomogeneities can be reliably detected in the training phase and then interactively used as salient features in the image segmentation phase. Hence, we enhance the segmentation model with *a priori* knowledge about natural variation and anatomical saliency in the visual appearance of the spine rather than focusing on more *a priori* geometrical or spatial knowledge.

The paper is organized as follows. In Section II related work on segmentation of spinal images is discussed. Section III briefly describes the image material used in this work and introduces the proposed method. The following issues are addressed: the necklace model for capturing vertebral structures,

Manuscript received October 9, 2002; revised February 14, 2004. *Asterisk indicates corresponding author.*

*S. Ghebreab was with the Intelligent Sensory Information Systems group, Informatics Institute, University of Amsterdam, Amsterdam 1098 SJ, The Netherlands. He is now with the Biomedical Imaging Group Rotterdam, Departments of Medical Informatics and Radiology, Erasmus MC, University Medical Center Rotterdam, Dr. Molewaterplein 50, 3015 GE Rotterdam, The Netherlands (s.ghebreab@erasmusmc.nl).

A. W. M. Smeulders is with the Intelligent Sensory Information Systems group, Informatics Institute, Faculty of Science, University of Amsterdam, Kruislaan 403, 1098 SJ Amsterdam, The Netherlands.

Digital Object Identifier 10.1109/TBME.2004.831540

the string model for expressing spinal curvatures and the spine model for segmenting the entire spine by elastic deformation in the image reminiscent of a marionette with interrelated structures moved by strings. In Section IV an illustration of the entire segmentation process is given. Discussion and conclusion follow in Section V.

II. Related Work

Image-based analysis of spinal morphology predominantly involves multiplanar images on which two-dimensional (2-D) segmentation models, e.g., [4] and [5] or 3-D segmentation models, e.g., [6] and [7], are applied. Here, we discuss a number of 3-D models for segmentation of 3-D spinal or vertebral images in terms of boundary model, objective function, model deformation and interaction.

In [8], an image segmentation model is proposed that uses prior knowledge of an object's structure to guide the search for its boundaries. The boundary model is a 3-D radial surface, which is a direct extension of the radial contour model [9] that has also been applied for interactive segmentation of vertebral structures. The surface is represented as a series of parallel slices, where the center points for the slices are collinear, forming an axis that runs perpendicular to all the slices. A realistic radial surface model of vertebral structures is constructed on the basis of a training set. The user instantiates a shape model for a given volume dataset by indicating a set of landmarks in the volume data. These landmarks define the model's local coordinate system within the image volume, and may also provide initial values for one or two radials. A constraint propagation algorithm is invoked to find the values for the remaining radials that are consistent with these starting points. The radial surface is deformed in the image to optimize an objective function such that in the result radials correspond with highlighted edges in the volume image. During segmentation, an uncertainty interval is maintained for each radial so as to keep track of which values still satisfy the constraints to maintain the trained shape of the model.

In [10] and [11], a more sophisticated model is introduced for segmentation of the cervical spine. The cervical spine model is a finite-element model augmented with additional structures to locate landmarks, contours, surfaces, and regions. The spine model is constructed on the basis of a training set of spinal images. This training set is fed to a tessellation algorithm and a smoothing and triangle decimation step to produce a typical set of triangular surface patches comprising each individual vertebra. The surfaces and volumes are used in statistical estimation modules to interactively localize a number of *a priori* selected landmarks in a new image, using the finite-element model as a road map. Once the landmarks are found they are successively employed to refine the vertebra models using a nonlinear optimization method that aims to minimize the distance of the model surface to the vertebra surface in the image. The objective function that drives the model deformation is based on gray-value intensity, image gradient and curvature properties. Other works that apply a finite element model for segmentation of spinal or vertebral structures include [12].

In [13] and [14], a method is presented which allows the development of a statistical shape model of an object's surface, in the reference these are vertebral surfaces. A statistical shape model is obtained from a training set by principal component analysis. For image segmentation, the average shape model is interactively placed in the image in the proximity of the vertebral structure of interest. To this end, mesh cut-lines of the average shape model are roughly positioned onto orthogonal cuts of a 3-D computed tomography (CT) image. The average model is then deformed in statistically feasible ways to find the vertebral boundary in the gray-level image. Model deformation reduces to optimization of the weights of the first principal eigenmodes and of the translational and rotational parameters. The statistical shape model is easily extended to capture multiple vertebrae, however, without the capacity to explicitly quantify properties of the entire spine. Other works that use a statistical shape model for segmentation of spinal or vertebral structures include [6]. Vrtovec *et al.* [15] propose a similar shape model incorporating gray-level information.

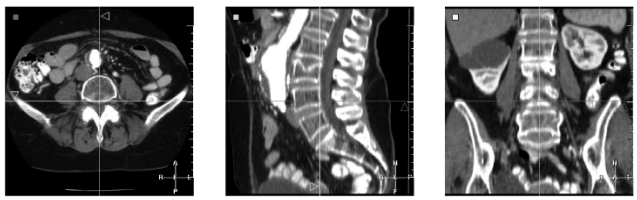

Fig. 1. From left to right: axial, sagittal, and coronal cross sections of a spinal CT image. The images reveal an infrarenal aortic aneurism, renal and oesteoporotic fracture of the plate only obvious on the sagittal reconstruction.

The reported methods have in common that an intrinsically 3-D boundary model is constructed from *a priori* information and then realistically deformed in a 3-D image using interactively defined and localized landmarks as a guide. However, with the exception of [15], the methods do not rely on *a priori* information about the gray-level appearance of vertebral structures. The gray-level informahas specific characteristics and is highly suited to enhance the segmentation model. Apart from this, most of the 3-D methods rely on manual definition and localization of anatomical landmarks, which is subjective and laborious. To overcome these shortcomings we propose an interactive statistical segmentation model of continuous image and shape features with automatically defined and interactively applied landmarks.

III. Materials and Method

We use image data consisting of CT scans of the abdomen of a group of 18 elderly people, originally taken to investigate the aorta (see Fig. 1). All subjects were scanned with a Philips SR 700 CT at 140 KV (Philips Medical Systems, Best, The Netherlands) using a maximum field of view (48 cm). Each CT image contains about 300 slices of 512×512 pixels. Slice thickness is 0.5 mm, slice interval is 0.5 mm and density resolution is 12 bits. CT source images have been transferred to an offline computer workstation (EasyScil, Philips Medical Systems) for viewing and post processing. We concentrate on the lower four lumbar vertebrae (L2, L3, L4, L5) and demonstrate our method on 6 CT images of subjects with minimal spinal and vertebral deformities.

For segmentation of the spine images we use deformable models (see, e.g., [16]–[18] for detailed information). First introduced by Kass *et al.* [19] and Staib *et al.* [20], the idea behind deformable models is to treat segmentation as an optimization

problem, typically by minimizing a model fitting function that rewards locally smooth boundaries passing through high-gradient image regions. A model is deformed in the image trying to compromise between features derived from the image and features obtained from a shape model. The deformation stops when an equilibrium is reached. The deformable model is then assumed to lie on the target boundary in the image.

We adopt the deformable model approach with the difference that we aim to learn vertebral features rather than to define them on the basis of *a priori* geometrical knowledge. In addition, to exploit salient and variational information as observed in a given training set of segmented spinal images we construct 1) models of the lumbar vertebrae using necklaces, 2) models of the spinal curvatures using strings, and 3) an integral spine model using coupled necklace and string models. In the following section we describe the models one by one.

A. Necklace Models of Vertebral Surfaces

The vertebra surface has many concave and convex surface parts differing from weakly to strongly curved. Analogous to diversity in surface shape, the gray-level structure along the vertebra boundary varies from one part to the other. At some parts the vertebra boundary has well-defined intensity discontinuities, while at other parts there is vague pictorial evidence and/or none at all due to insufficient image quality or interfering structures in the neighborhood.

To appropriately capture and exploit the locally sophisticated shape and gray-level appearance of the vertebra surface we need to observe multiple features. For this reason, we employ necklaces [3]. A necklace model allows for the analysis of inhomogeneous boundaries by recording a repertoire of shape and gray-level features along a continuous surface. Specifically it allows for exploitation of salient features as landmarks for image segmentation.

1) Surface Representation: The appearance of the spine is learned from a set of $M = 5$ training objects, consisting of 3-D spinal images $I_m : \mathbf{x} \in \Re^3 \rightarrow \Re, m = 1, \ldots, M$ and ground-truth vertebral surface $\mathbf{s}_m^\vartheta : \mathbf{u} \in \Re^2 \rightarrow \Re^3, \vartheta = 1, \ldots, V$, one for each vertebra. In order to optimally represent the continuous vertebral surface we use continuous B-spline surfaces. The advantage of a B-spline representation is that quantitative information can be analytically computed, allowing for more complete and accurate measurements. The B-spline surface is a collection of B-Spline curves [21], i.e., the vertebral surface is defined as the set of all points given by the following expression for all parameter values of $\mathbf{u} = [u_1, u_2]^T$:

$$\mathbf{s}(\mathbf{u} \,|\, \mathbf{b}^{i,j}) = \sum_{i=0}^{I} \sum_{j=0}^{J} B_p^i(u_1) B_q^j(u_2) \mathbf{b}^{i,j} \tag{1}$$

where $\mathbf{b}^{i,j}$ is the array of $I \times J$ control points. The $B_p^i(u_1)$ are B-spline basis functions of degree $p-1$ in u_1 direction, which are $p-2$ times continuously differentiable. The $B_q^j(u_2)$ are the basis functions of degree $q-1$ in u_2, which are $q-2$ times continuously differentiable. A set of knots in a path parameter interval relating to the control points is used to define the basis functions. For an analytic expression of B-splines basis functions see [21].

We control the B-spline surface by interpolation points $\mathbf{p}^{\imath,\jmath}$ rather than by control points $\mathbf{b}^{i,j}$. This is beneficial because a restricted number of points are required to define the spine and to control the spine model when defining ground-truth surfaces and when segmenting images. Here, the ground-truth vertebra surface is obtained by interpolating a B-Spline surface through 12×12 interpolation points using centripetal surface parametrization to handle very sharp turns [21]. The interpolation points are defined as

$$\mathbf{p}^{\imath,\jmath} = \mathbf{s}\left(u_1^\imath, u_2^\jmath\right) = \sum_{i=1}^{I} \sum_{j=1}^{J} B_p^i\left(u_1^\imath\right) B_q^j\left(u_2^\jmath\right) \mathbf{b}^{\imath,\jmath}. \tag{2}$$

The interpolation points are indicated by a medical expert in three 2-D orthogonal slices of the volume data once and within one day. Generally, the interpolated B-spline surface corresponds to the true vertebral surface. At places where the B-spline surface locally deviates from the true vertebra surface, better correspondence can be obtained either by indicating boundary points more precisely or more densely.

2) Feature Definition: After construction of the ground-truth B-spline vertebra surfaces, they are manually aligned to prepare them for statistical analysis. Manual alignment reduces to indicating corresponding landmark points on the different vertebra surfaces in our training set. Once the B-spline surfaces are aligned and validated by visual inspection, shape and image features are sampled at 400 points and conveniently captured by feature function $\mathbf{f}_m^\vartheta(\mathbf{u})$ in the N-dimensional functional space. The functional $\mathbf{f}_m^\vartheta(\mathbf{u})$ is a manifold defined as the B-spline surface that interpolates through the sampled features. Considering the ϑth vertebrae, the set of multivariate continuous features deduced from the training data by the mapping $\mathbf{f}^\vartheta : \mathbf{u} \in \Re^2 \rightarrow \Re^N$ is then represented by

$$\mathbf{F}^\vartheta(\mathbf{u}) = \left[\mathbf{f}_1^\vartheta(\mathbf{u}), \ldots, \mathbf{f}_M^\vartheta(\mathbf{u})\right]. \tag{3}$$

Here, we have chosen to compute the location, rotation and scale invariant *mean curvature* as the first local shape feature to be recorded along the surface outlines. This feature is captured by $f_{m3}^\vartheta(\mathbf{u})$. We also compute the principal curvatures to simplify landmark definition in subsequent steps. They are captured in $f_{m3}^\vartheta(\mathbf{u})$ and $f_{m2}^\vartheta(\mathbf{u})$, respectively. The feature values are analytically computed from the B-spline surfaces $\mathbf{s}_m^\vartheta(\mathbf{u})$ and are then used to construct feature functions $\mathbf{f}_m^\vartheta(\mathbf{u})$ by interpolating smooth B-spline surface through them. Table I lists the shape feature definitions.

TABLE I
SHAPE FEATURES IN OUR IMPLEMENTATION. FIRST PRINCIPAL CURVATURE VALUES $f_{m1}^\vartheta(\mathbf{u} \,|\, \mathbf{S}_m)$ FORM THE FIRST DIMENSION OF THE FUNCTIONAL SPACE AND SECOND PRINCIPAL CURVATURE VALUES $f_{m2}^\vartheta(\mathbf{u} \,|\, \mathbf{S}_m)$ FORM THE SECOND DIMENSION. THE THIRD DIMENSION IS FORMED BY SCALE INDEPENDENT *MEAN CURVATURE* VALUES $f_{m3}^\vartheta(\mathbf{u} \,|\, \mathbf{S}_m)$

Feature	Dimension	Definition
1st princ. curvat.	$f_{m1}^\vartheta(\mathbf{u}\|\mathbf{s}_m^\vartheta)$	$k_1(\mathbf{u}\|\mathbf{s}_m)$
2nd princ. curvat.	$f_{m2}^\vartheta(\mathbf{u}\|\mathbf{s}_m^\vartheta)$	$k_2(\mathbf{u}\|\mathbf{s}_m)$
mean curvature	$f_{m3}^\vartheta(\mathbf{u}\|\mathbf{s}_m^\vartheta)$	$\frac{(k_1(\mathbf{u}\|\mathbf{s}_m^\vartheta) * k_2(\mathbf{u}\|\mathbf{s}_m^\vartheta))}{\delta A(\mathbf{u}\|\mathbf{s})}$

Following [3], we also compute the three image features listed in Table II. They are obtained from the structure tensor matrix $\mathbf{M}(\mathbf{x};\sigma)$ [22]. This matrix gives for each image point $\mathbf{x}$ the local 3-D structure of the image at scale σ. When all its eigenvalues are sufficiently large this indicates a point-like structure. Feature function $f_{m4}^\vartheta(\mathbf{u} \,|\, I_m, \mathbf{s}_m^\vartheta)$ expresses such point-like structures. Two eigenvalue, λ_1, λ_2, a multitude larger than the smallest eigenvalue λ_3 indicates a point on a curve-like

TABLE II
IMAGE FEATURES IN OUR IMPLEMENTATION: $f^{\vartheta}_{m4}(\mathbf{u}\,|\,I_m,\mathbf{s})$ HIGHLIGHTS POINT LANDMARKS, $f^{\vartheta}_{m5}(\mathbf{u}\,|\,I_m,\mathbf{S}_m)$ HIGHLIGHTS CURVE LANDMARKS, $f^{\vartheta}_{m6}(\mathbf{u}\,|\,I_m,\mathbf{S}_m)$ HIGHLIGHTS SHEET POINTS

image point landmarks	$f^{\vartheta}_{m4}(\mathbf{u}\|I_m,\mathbf{s}^{\vartheta}_m)$	$1-e^{-\frac{\lambda_3}{c_t}}$
image curve landmarks	$f^{\vartheta}_{m5}(\mathbf{u}\|I_m,\mathbf{s}^{\vartheta}_m)$	$1-e^{-\frac{\lambda_2}{c_t}}$
image sheet points	$f^{\vartheta}_{m6}(\mathbf{u}\|I_m,\mathbf{s}^{\vartheta}_m)$	$1-e^{-\frac{\lambda_1}{c_t}}$

structure. This is expressed by $f^{\vartheta}_{m5}(\mathbf{u}\,|\,I_m,\mathbf{s}^{\vartheta}_m)$. Finally, feature function $f^{\vartheta}_{m6}(\mathbf{u}\,|\,I_m,\mathbf{s}^{\vartheta}_m)$ highlights sheet-like structures. The distinction between the three types of surface points is made on the basis of the normalization constant c_t, reflecting the minimum required image variation for an image point to be classified as point or curve landmark. This way we can focus on strong point landmarks and curve landmarks while disregarding image variations caused by minor bumps or noise.

The extraction of $N = 6$ features for each vertebra yields $M = 5$ sets of $V = 4$ surfaces in a 6-dimensional functional space. These surfaces are statistically analyzed for model construction.

3) Landmark Selection: We aim at exploiting landmarks that are defined by the multiple features recorded along the continuous vertebra surface. Thanks to the B-spline surface representation, no manual or other additional heuristic techniques are required to compute the positions of landmarks, in contrast with other approaches such as [4]. Vertebral landmark definition reduces to localizing peaks in feature function values $\mathbf{f}^{\vartheta}_m(\mathbf{u})$. However, rather then separately investigating each training instance m for landmarks, we first compute the elementary statistics of the training sets. Then we try to identify robust landmarks from the average feature functions. The population average for vertebra ϑ is computed as

$$\bar{\mathbf{f}}^{\vartheta}\left(\mathbf{u}\,\middle|I_m,\mathbf{s}^{\vartheta}_m\right)=\frac{1}{M}\sum_{m=1}^{M}\mathbf{f}^{\vartheta}_m\left(\mathbf{u}\,\middle|I_m,\mathbf{s}^{\vartheta}_m\right). \tag{4}$$

The functional $\bar{\mathbf{f}}^{\vartheta}(\mathbf{u})$ is a surface in the N-dimensional functional space, obtained by averaging each training surface $\mathbf{f}^{\vartheta}_m(\mathbf{u}\,|\,I_m,\mathbf{s}_m)$ in each dimension. The corresponding standard deviation is

$$\boldsymbol{\sigma}_{\mathbf{f}^{\vartheta}}\left(\mathbf{u}\,\middle|I_m,\mathbf{s}^{\vartheta}_m\right)=\left(\frac{1}{M-1}\sum_{m=1}^{M}\left\|\mathbf{f}^{\vartheta}_m\left(\mathbf{u}\,\middle|I_m,\mathbf{s}^{\vartheta}_m\right)-\bar{\mathbf{f}}^{\vartheta}(\mathbf{u})\right\|^2\right)^{1/2}. \tag{5}$$

The average feature function $\bar{\mathbf{f}}^{\vartheta}(\mathbf{u})$ is investigated for high curvature points on the basis of its local second order properties [23]. These properties are obtained from the infinite set of planes passing through and containing the normal in geometric space at a specific point on the population average surface $\bar{\mathbf{f}}^{\vartheta}(\mathbf{u})$. For example, when the only features considered are the x, y, and z coordinates of the vertebral surfaces $\mathbf{s}^{\vartheta}_m(\mathbf{u})$, each of the normal planes intersects the surface by a planar curve. The curvature at the point of interest is an identifying curvature measure for the surface. The pair of directions $\mathbf{v}$ and $\mathbf{w}$ are defined such that these curvatures reach their maximum and minimum curvatures

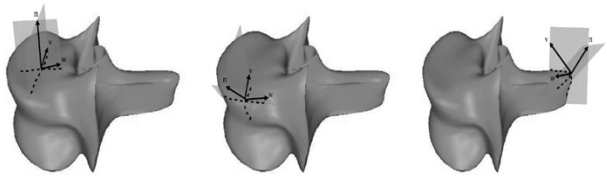

Fig. 2. Surface point properties are derived from the curves defined by the intersection of the surface with the two orthogonal planes that go through that point and contain the normal vector $\mathbf{n}$. The curves with minimal and maximal principal curvatures in corresponding directions $\mathbf{v}$ and $\mathbf{w}$ define the type point: sheet points have low bending and freedom to move in two directions (left), curve landmark have a fixed position in all but one dimension (middle) point landmark have no free dimensions and are precisely localized (right).

κ_1 and κ_2 as illustrated in Fig. 2. We use these principal curvatures and locally associated directions to define landmarks.

We make a distinction between point landmarks, curve landmarks and sheet points by evaluating the principal curvature values at each point of $\bar{\mathbf{f}}^{\vartheta}(\mathbf{u})$. Point landmarks are surface points $\mathcal{U}_A$ where both principle curvatures have an extreme absolute value. They are precisely localized in three dimensions. Surface points where the absolute value of one of the principal curvatures is extreme, are curve landmarks, denoted by $\mathcal{U}_B$. They are precisely localized in two dimensions. At sheet points $\mathcal{U}_C$ both values of the absolute principle curvature is low. Typically they are well-defined in only one dimension. The sets $\mathcal{U}_A$,$\mathcal{U}_B$,$\mathcal{U}_C$ together contain all relevant path positions. A threshold for the principal curvature values may be chosen such that the definition of these sets, i.e., the distribution of geometrical surface landmarks, largely coincides with anatomical landmarks.

At this point we have $V = 4$ necklace models: one for each vertebra. In the segmentation step, the information contained in $\bar{\mathbf{f}}^{\vartheta}(\mathbf{u})$ and $\boldsymbol{\sigma}_{\mathbf{f}^{\vartheta}}(\mathbf{u})$ is used as a reference model for feature selection and qualification. The sets $\mathcal{U}_A$,$\mathcal{U}_B$,$\mathcal{U}_C$ are used for landmark-based segmentation.

B. String Models of the Spinal Curves

We stack each of the necklace models to obtain a model at the level of the spine. The stack of necklace models allows us to model the cervical and lumbar curvatures, characterized by a convex shape, and the thoracic and sacral curvatures, characterized a convex forward shape. These spinal curvatures are almost always present with some variation across and among subjects. A model of these curvatures, therefore, is likely to assist segmentation of the spine in an image.

We aim at capturing the spinal curvatures using string models. As introduced in [2], in contrast to other similar approaches (e.g., [24]–[26]), the string model has the capacity to build a detailed underlying statistical model of open and closed boundaries from multiple continuous shape and image features. Here, we use strings to catch the common appearance of the spinal curvatures observed in our training data and the main modes of variation therein, in ways similar to [27].

1) Curve Representation: The shape of the spinal curvatures is learned from the same training set of $M = 5$ example images and $V = 4$ surface outlines described in Section III-A. Assuming the landmarks on the lumbar vertebrae occur at approximately the same position, we select point landmarks $\mathbf{u}_\ell \in \mathcal{U}_A$ for $\ell = 1,\ldots,L$ and learn the appearance of the L curves that pass through the surface landmark points

TABLE III
CURVE FEATURES IN OUR IMPLEMENTATION. THE FUNCTIONAL $f^{\ell}_{m1}(u \mid I_m, \mathbf{c}^{\ell}_m)$ EXPRESSES THE CONTOUR CURVATURE, COMPUTED ON THE BASIS OF FIRST DERIVATIVE $\dot{\mathbf{c}}$ AND SECOND DERIVATIVE $\ddot{\mathbf{c}}$. THE FUNCTIONAL $f^{\ell}_{m2}(u \mid I_m, \mathbf{c}^{\ell}_m)$ CAPTURES THE IMAGE GRADIENT

Feature	Dimension	Definition
curvature	$f^{\ell}_{m1}(u\|I_m, \mathbf{c}^{\ell}_m)$	$\frac{\|\|\dot{\mathbf{c}}^{\ell}_m(u)\times\ddot{\mathbf{c}}^{\ell}_m(u)\|\|}{\|\|\dot{\mathbf{c}}^{\ell}_m(u)\|\|^{3/2}}$
gradient	$f^{\ell}_{m2}(u\|I_m, \mathbf{c}^{\ell}_m)$	$\nabla I(\mathbf{c}^{\ell}_m(u))$

$\mathbf{s}^1_m(\mathbf{u}_\ell), \ldots, \mathbf{s}^V_m(\mathbf{u}_\ell)$. We represent the ℓth curve in the mth training image by a qth-order tensor product B-spline curve that handles the mapping $\mathbf{c} : u \in \Re \rightarrow \Re^3$. The B-spline curve is defined by

$$\mathbf{c}^l_m(u; \mathbf{p}^v) = \sum_{v=1}^{V} B^v_q(u)\mathbf{p}^v. \tag{6}$$

Basis functions $B^v_q(u)$ correspond to the $V = 4$ interpolation points $\mathbf{p}^v$. This way, each curve captures the spatial relation between corresponding point landmarks on adjacent vertebrae, derived automatically from the vertebral surfaces $\mathbf{s}^{\vartheta}_m(\mathbf{u})$.

2) Feature Definition: Image and shape features are extracted along the curves $\mathbf{c}^{\ell}_m(u)$ in the training set and captured by space curves in functional space. This yields the set of feature functions

$$\mathbf{F}^{\ell}(u) = \left[\mathbf{f}^{\ell}_1(u), \ldots, \mathbf{f}^{\ell}_M(u)\right]. \tag{7}$$

We observe two features along the curve $\mathbf{c}^{\ell}_m(u)$. The first feature is the 3-D curvature, which is analytically computed at each point of $\mathbf{c}^{\ell}_m(u)$. We have chosen this feature because of its invariance properties and because it might reveal new and interesting anatomical knowledge. For example, the value and location of the maximum curvature along the spinal curves has already been reported to be a relevant clinical measure for spinal deformities [27]. Curvature values are computed entirely in 3D. The second feature measures the image gradient magnitude, supporting the definition of spinal curvature by means of image evidence, which is mainly confined at tips of the vertebral structures. Table III lists the two features and their definition.

The extraction of two features for each spinal curvature yields $M = 5$ sets of $L = 6$ curves in a 2-D functional space, to be analyzed statistically for model construction.

3) Variational Information: We aim at statistically modeling the natural variability of the spinal curvatures in terms of shape and gray-level features. This differs from the mainstream methods in that we do not define spinal curvatures on the basis of *a priori* geometrical knowledge such as smoothness on intra- and inter-curve properties of the spine [28]. Learning the common appearance of the spinal curvatures allows us to base the search criteria for model deformation on natural variations. The elementary statistics from our training data are summarized by average

$$\bar{\mathbf{f}}^{\ell}\left(u \left| I_m, \mathbf{c}^{\ell}_m\right.\right) = \frac{1}{M}\sum_{m=1}^{M} \mathbf{f}^{\ell}_m\left(u \left| I_m, \mathbf{c}^{\ell}_m\right.\right). \tag{8}$$

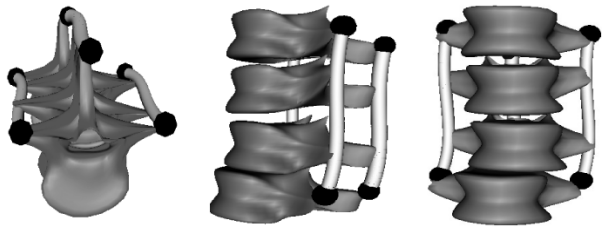

Fig. 3. The integral spine model from three different perspectives: axial (left) sagittal (middle) and coronal (right). It consists of multiple necklace models for vertebrae coupled by string models as in a marionette.

The one-dimensional (1-D) curve $\bar{\mathbf{f}}^{\ell}(u)$ in the multidimensional functional space is obtained by averaging each training curve $\mathbf{f}^{\ell}_m(u)$ in each dimension separately. The standard deviation is

$$\boldsymbol{\sigma}_{\mathbf{f}^{\ell}}(u) = \left(\frac{1}{M-1}\sum_{m=1}^{M}\left\|\mathbf{f}^{\ell}_m\left(u \left| I_m, \mathbf{c}^{\ell}_m\right.\right) - \bar{\mathbf{f}}^{\ell}(u)\right\|^2\right)^{1/2} \tag{9}$$

The average feature function $\bar{\mathbf{f}}^{\ell}(u)$ and variation $\boldsymbol{\sigma}_{\mathbf{f}^{\ell}}(u)$ only contain elementary statistics of the training data. Variational information is captured in more detail by functional data analysis [29], producing string models of the spinal curvatures. The string models capture the most important modes of variation by functional principal components analysis. In addition, they incorporate a functional principal regression model that allows to weight features according to these modes of variation and to explain unknown instances by a statistically determined feature weighting procedure. We refer to [2] for more detail.

At this point we have a detailed statistical description of the spinal curvatures. For simplicity, we assume all the relevant information is contained in $\bar{\mathbf{f}}^{\ell}(u)$, and $\boldsymbol{\sigma}_{\mathbf{f}^{\ell}}(u)$. We proceed with only these two quantities. The tubes in Fig. 3 illustrates the population average spinal curvatures of the spinal lumbar parts in our training data.

C. A Deformable Integral Spine Model

To form an integral model of the spine we couple the necklace models of vertebrae and the string models of the spinal curvature as illustrated in Fig. 3. The spine model is deformed onto new image data such that it fits best the spine visualized by that image.

1) Qualification: The *deformable integral spine model* consists of deformable surfaces $\mathbf{s}^{\vartheta}_t(\mathbf{u})$ and deformable curves $\mathbf{c}^{\ell}_t(u)$, which account for variability among vertebral structures and their interrelationships, respectively. For all $V = 4$ necklace models, the initial surfaces are $\mathbf{s}^{\vartheta}_{t=0}(\mathbf{u})$ and curve $\mathbf{c}^{\ell}_{t=0}(u)$ and for all $L = 6$ string models the initial curves are the population average. That is, assuming models $\mathbf{s}^{\vartheta}_m(\mathbf{u})$ and $\mathbf{c}^{\ell}_m(u)$ are properly aligned and uniformly parameterized to establish point correspondence the initial models are defined as

$$\mathbf{s}_{t=0}(\mathbf{u}) = \frac{1}{M}\sum_{m=1}^{M}\mathbf{s}^{\vartheta}_m(\mathbf{u}) \tag{10}$$

$$\mathbf{c}_{t=0}(u) = \frac{1}{M}\sum_{m=1}^{M}\mathbf{c}^{\ell}_m(u). \tag{11}$$

The fit quality is determined on the basis of features $\mathbf{f}^{\vartheta}_t(\mathbf{u})$ and $\mathbf{f}^{\ell}_t(u)$ emanating from $\mathbf{s}^{\vartheta}_{t=0}(\mathbf{u})$ and $\mathbf{c}^{\ell}_{t=0}(u)$ respectively.

The model fitting function is a compromise between the fit quality of the necklace models and the string models. When the set $\mathbf{s}_t^1(\mathbf{u}),\ldots,\mathbf{s}_t^V(\mathbf{u})$ is represented by $\mathbf{S}_t(\mathbf{u})$ and $\mathbf{c}_t^1(u),\ldots,\mathbf{c}_t^L(u)$ by $\mathbf{C}_t(u)$ we have

$$\Theta_{\text{spine}}(\mathbf{S}_t(\mathbf{u}),\mathbf{C}_t(u)) = \frac{1}{V}\sum_{\upsilon=1}^{V}\omega^{\vartheta}\cdot\theta^{\vartheta}\left(\bar{\mathbf{f}}^{\vartheta},\boldsymbol{\sigma}_{\mathbf{f}^{\vartheta}},\mathbf{f}_t^{\vartheta}\right) + \frac{1}{L}\sum_{l=1}^{L}\omega^{\ell}\cdot\theta^{\ell}\left(\bar{\mathbf{f}}^{\ell},\boldsymbol{\sigma}_{\mathbf{f}^{\ell}},\mathbf{f}_t^{\ell}\right). \quad (12)$$

The first term measures the distance between the expected and the sampled values for each vertebra ϑ. To ensure a controllable distance measure, the Mahalanobis distance [30] is computed using mean and variation information obtained from the training data. For the ϑth vertebra this means

$$\theta^{\vartheta}\left(\mathbf{s}_t^{\vartheta}(\mathbf{u})\left|\bar{\mathbf{f}}^{\vartheta},\boldsymbol{\sigma}_{\mathbf{f}_t^{\vartheta}},\mathbf{f}^{\vartheta}\right.\right) = \int_{\mathbf{u}}\upsilon(\mathbf{u})\left\|\frac{\bar{\mathbf{f}}^{\vartheta}(\mathbf{u})-\mathbf{f}_t^{\vartheta}(\mathbf{u})}{\boldsymbol{\sigma}_{\mathbf{f}^{\vartheta}}(\mathbf{u})}\right\|^2 d\mathbf{u}. \quad (13)$$

The fit is controlled by means of the function $\upsilon(\mathbf{u})$ which weights the fit at each point of the deformable surface $\mathbf{s}_t^{\vartheta}(\mathbf{u})$. Weighting is done according to the type of surface point under consideration: for point landmarks there is a predefined weight υ_A, for curve landmarks υ_B and for sheet points υ_C. For example, interactive landmark-based image segmentation is performed using settings $\upsilon_A = 1, \upsilon_B = 0, \upsilon_C = 0$. The weights may also be set such that features along the entire surface contribute by setting all values larger than 0, but are constrained to add up to one.

The second component in (12) measures the distance between the expected and the sampled values for each of the $L = 6$ modeled spinal curvatures. This way the deformable integral spine model seeks resemblance between the reference spinal curvature $\mathbf{f}^{\ell}$ and the deformed curve $\mathbf{f}_t^{\ell}$ normalized by the common modes of variation. For the ℓth string model the fit quality is formulated as

$$\theta^{\ell}\left(\mathbf{C}_t^{\ell}(u)\left|\bar{\mathbf{f}}^{\ell},\boldsymbol{\sigma}_{\mathbf{f}^{\ell}},\mathbf{f}_t^{\ell}\right.\right) = \int_{u}\left\|\frac{\bar{\mathbf{f}}^{\ell}(u)-\mathbf{f}_t^{\ell}(u)}{\boldsymbol{\sigma}_{\mathbf{f}^{\ell}}(u)}\right\|^2 du. \quad (14)$$

The model fitting function is regulated by means of weights ω^{ϑ} and ω^{ℓ}, which are positive and add up to one. Their value is defined by the user and generally tuned such that they emphasis either the fit of the necklace models or the fit of the strings models. The fit quality forms the basis for optimization.

2) Optimization: Having specified the model fitting function, we must choose how to optimize the degrees of freedom of the deformable integral spine model. The degrees of freedom are specified by the number and types of points that control the spine model. Each of the $V = 4$ necklace models is controlled by 12×12 interpolation points (see Fig. 4). We, thus, have a total of 448 control points which we need to reposition in order to optimize the spine model. Optimization of the spine model is done progressively: a single necklace model is optimized and fixed, results are propagated to the remaining necklace models via the string models, the next adjacent necklace model is refined and fixed and results are propagated to the remaining necklace models, etc. Optimization only effects the surface geometry of the necklace models: in our implementation the curves constituting the string models are automatically derived from them.

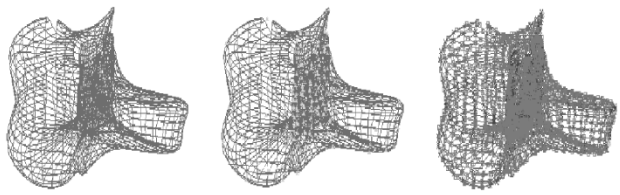

Fig. 4. A wire-frame representation of the vertebral surface. Left: the sample points are the intersection points of the wire-frames. Middle: the interpolation points are a subset of the sample points (green). Right: classification of the sample points into point landmarks (green), curve landmarks (blue) and sheet points (purple). The six points designated for user interaction are a subset of the point landmarks.

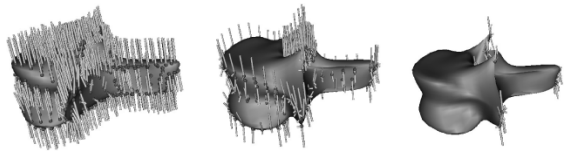

Fig. 5. For each type of surface point the search area is specified in terms of local surface properties. Left: sheet points are optimized in the normal direction (small stripes indicate the direction at each sheet point) perpendicular to the surface. Middle: curve landmarks in a 2-D area spanned by the normal and first principal direction. Right: point-landmarks in a 3-D area specified by the normal and principal directions.

We discuss optimization of a necklace model and propagation of its results via string models to obtain the optimal spine model

$$\Theta_{\text{spine}}^{\text{optimal}} = \arg\min_{\mathbf{S}_t^{\vartheta},\mathbf{C}_t^{\vartheta}}\Theta_{\text{spine}}(\mathbf{S}_t,\mathbf{C}_t). \quad (15)$$

Optimization of a single necklace model involves two main steps. In the first step, a new position is suggested for an interpolation point on the necklace model and the model fitting function value is recomputed for the spine model. This is followed by deformation of the necklace model to move the point to the newly suggested position if the model fits better this way. Interpolation points are optimized either in a 3-D, 2-D, or 1-D space, depending on the type of surface points: point landmarks are optimized in three dimensions, curve landmarks in two dimensions, and sheet points in one dimension. The 3-D search space is defined by a linear combination of the vectors $\mathbf{n}, \mathbf{v}$, and $\mathbf{w}$ as defined in Fig. 5. The 2-D search space is defined by a linear combination the vectors $\mathbf{n}$ and $\mathbf{v}$. The 1-D search space is defined by $\mathbf{n}$. Optimizing a point landmark, for example, reduces to finding optimal values for scalars α, β, and γ that define the point movement

$$\mathbf{d}\left(\mathbf{u}\left|\mathbf{s}_t^{\vartheta}\right.\right) = \alpha\mathbf{n}\left(\mathbf{u}\left|\mathbf{s}_t^{\vartheta}\right.\right) + \beta\mathbf{v}\left(\mathbf{u}\left|\mathbf{s}_t^{\vartheta}\right.\right) + \gamma\mathbf{w}\left(\mathbf{u}\left|\mathbf{s}_t^{\vartheta}\right.\right). \quad (16)$$

Apart from the differences in degrees of freedom per surface point, we also differentiate between priority per surface point. The following scheme is employed: 1) optimize point landmarks on the necklace model in a 3-D area, resulting in a rough estimate of the position of the vertebra boundary by its point landmarks; 2) optimize curve landmarks in a 2-D area departing from 1), resulting in the location of surface curve points determining the outline of the vertebrae; 3) optimize sheet points in a 1-D area departing from 2), resulting in the location of all boundary points; and 4) optimize all points one more time in their respective dimensions departing from 3) to fine tune the result and to obtain a global optimum. This scheme allows us to interactively search for a limited set of well-defined points in

the image and then to exploit solutions thereof to constrain the deformation of the entire necklace model.

We also distribute the force working on a point landmark to the entire necklace model. That is, we preserve the shape of the deformable surface as much as possible when fitting a specific surface point by simultaneously estimating the correct position for deformable surface points that have not yet been optimized. This means that, given drive $\mathbf{d}(\mathbf{u}_i \,|\, \mathbf{s}_t^{\vartheta})$ working on surface point $\mathbf{s}_t^{\vartheta}(\mathbf{u}_i)$, the following movement of points $\mathbf{s}_t^{\vartheta}(\mathbf{u}_j),\ \forall \mathbf{u}_j \in U$ is performed to compute

$$\mathbf{s}_{t+1}^{\vartheta}(\mathbf{u}_j) = \mathbf{s}_t^{\vartheta}(\mathbf{u}_j) + \mathbf{d}\left(\mathbf{u}_i \,\middle|\, \mathbf{s}_t^{\vartheta}\right) e^{-(\delta_s/c_d)} \tag{17}$$

where $\delta_s = D(\mathbf{s}_t^{\vartheta}(\mathbf{u}_i), \mathbf{s}_t^{\vartheta}(\mathbf{u}_j))$ denotes the Euclidean distance between surface points $\mathbf{s}_t^{\vartheta}(\mathbf{u}_i)$ and $\mathbf{s}_t^{\vartheta}(\mathbf{u}_j)$. The constant $c_d > 0$ is a predefined value controlling the magnitude of the distribution.

Optimization of a single necklace model effects adjacent necklace models by propagating the deformation of one necklace model to the others via the string models. That is, in searching for a specific vertebra we also estimate the position of other vertebrae. We do the estimation only when optimizing point landmarks so that only movement of one point landmark effects the entire spine model. We accomplish this by distributing the force that works on a single point on one necklace model to all other points on all necklace models, in this case, weighted according to distance. For example, if there is a drive $\mathbf{d}(\mathbf{u}_i)$ working on surface point $\mathbf{s}_t^{\vartheta}(\mathbf{u}_i), \mathbf{u}_i \in \mathcal{U}_A$, which is also the connection point $\mathbf{c}_t^{\ell}(u_i)$ for a string model, this yields the following estimation for $\mathbf{s}_t^{\vartheta}(\mathbf{u}_j)$ for all other necklace models $\vartheta = 1, \ldots, V$

$$\mathbf{s}_{t+1}^{\vartheta}(\mathbf{u}_j) = \mathbf{s}_t^{\vartheta}(\mathbf{u}_j) + \mathbf{d}(\mathbf{u}_i) e^{-(\delta_C/c_d)}. \tag{18}$$

The distance $\delta_C = D(\mathbf{c}_t^{\ell}(u_i), \mathbf{c}_t^{\ell}(u_j))$ between points $\mathbf{c}_t^{\ell}(u_i)$ and $\mathbf{c}_t^{\ell}(u_j)$ is used to determine the extent of the distribution. Here too, a small value for the distribution constant c_d influences the shape of the deformable necklace model above or beneath the one being optimized, while a large value also effects the shape of the surfaces at large distances. This way segmentation of a single vertebra influences the entire spine model.

IV. Application

We illustrate interactive segmentation of part of the Lumbar spine from a CT image that was excluded from the training data. First the fourth lumbar vertebra is segmented using a necklace model, then part of the lumbar spine is segmented with help of the spine model.

For initialization of the necklace model in the image data in the vicinity of the L4, a fixed point is selected to enable a quick correspondence between the model and the target boundary. The necklace model is interactively bootstrapped by pointing and clicking at the corresponding point in the image. In this segmentation session no translation, rotation or scaling is required as the initialization by point correspondence results in an acceptable starting point for the necklace model. The first row in Fig. 6 shows the condition after initialization from three different perspectives, with the image data rendered with opacity 0.5 and the model in it with opacity 1. The local fit quality at a number of control points is indicated with colored spheres. The color varies from green, indicating a good fit to red, expressing a bad fit. The local fit quality, in this case, is evaluated by measuring the distance of the features measured at that point of the necklace model to the corresponding features observed in the training set [see (12)].

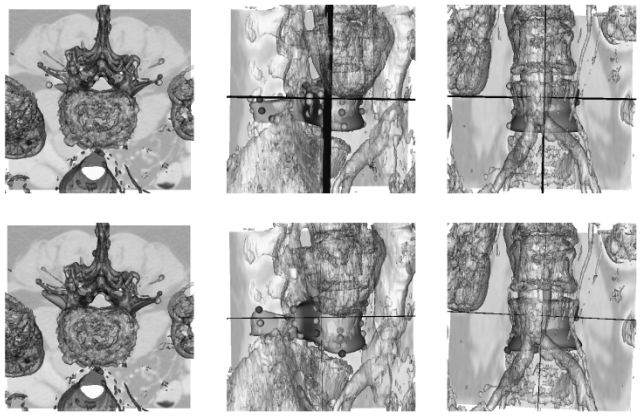

Fig. 6. The segmentation scene for three different perspectives. The image data is rendered transparently and the deformable model in it opaquely. First row: the initial necklace model. Second row: the deformation result.

Following the priority scheme described in the previous section, in the first step point landmarks are automatically fit to the image data after interactive marking of their approximate position. The following point landmarks are used for human-computer interaction: two points corresponding to the two tips on the spinal process, and the two tips at the two transverse processes. This produces a preliminary solution which is closer to the target boundary than was the starting condition. In the second step, curve landmarks, in particular at the lower part of the vertebral body, move toward the target boundary. In the third step, the lower and the upper planes of the vertebral body are reasonably found by deformation of the surface in one dimension. The result after optimizing all surface points once again in their respective dimension is illustrated in the second row of Fig. 6. In this case, the necklace model has found an optimal solution. The majority of the surface points is fitted well to the target vertebra. At some parts the necklace model moves away due to attraction by neighboring structures or due to locally too much deviation of the target boundary from the population average. A validation of the necklace model on CT images of vertebrae is given in [3].

To illustrate how the spine is segmented using the spine model, segmentation of part of the lumbar spine is performed. First the $L3$ is segmented by deformation of the corresponding deformable surface as before. Simultaneously, the position of the $L4$ is estimated by changing the geometry of the corresponding deformable surface according to the solution for the $L3$. On the basis of the preliminary solution for the $L4$, point landmarks on the $L4$ are sought under the constraints that the expected spatial relation is maintained as much as possible, i.e., spinal curvatures comply to the statistics. No interaction is required as the spine model is accurate enough to find the desired solution from that position. Then curve landmarks and sheet points are sought in the image data. The position of the initial deformable surfaces and curves and their position after optimizing are illustrated in Fig. 7. The step-by-step automatic segmentation of the $L3$ and $L4$ succeeds reasonably despite the articulated vertebral structures and their complex interrelationship.

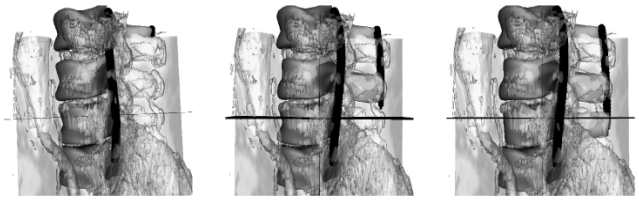

Fig. 7. Landmark-based segmentation of the third and fourth lumbar vertebrae. The spine model is visualized together with gray-level planes through the original image and transparent renderings of the high intensity objects: initial condition (left), condition after fitting the third lumbar necklace model (middle) and condition after fitting the fourth lumbar necklace model (right).

V. Discussion and Conclusion

We accentuate some important issues of our method. First, our method works completely in three dimensions, allowing to measure truly 3-D properties of vertebral structures and spinal curvatures, rather than relying on 2-D features. Second, we capture not only shape properties but also image properties as they also define the appearance of the spine. Multiple continuous features are extracted, then statistically analyzed by multivariate functional techniques [29] to obtain subtle but important population statistics. This is done 1) to exploit natural patient-to-patient variation of the spine appearance for constraining the deformation of the spine model and 2) to exploit salient information, defined as differential geometrical multifeature surface landmarks, for reducing the complexity of the image segmentation problem. Furthermore, we do a step-by-step interactive image segmentation departing from geometrically well-defined landmarks on a particular vertebra rather than a one shot integral solution for the spine using manually marked anatomical landmarks. We incrementally and elastically deform the spine model in the image reminiscent to a marionette with interrelated structures moved by strings.

We have illustrated how interactive CT image segmentation of the spine is facilitated using the integral deformable spine model. The segmentation was of exemplary nature, showing only the essential concept of our method. Clearly, a larger image data set with more accurate ground-truth segmentation is required to asses the accuracy of the method and its usefulness for clinical use, e.g., using statistically large number of spine images with ground-segmentations such as in [6] and [15]. Large training sets are both crucial and viable for construction and validation of accurate statistical image segmentation models. For further validation a particular interest is in the long term goal of analyzing average and variation characteristics of normal spines from longitudinal studies [1], in ways similar to [27] and [31], for the purpose of calculation of local and global deformity quantifying parameters.

We note that we have only considered CT images of normally appearing spine. When dealing with spinal deformities such as scoliotic spines that exhibit lateral curvatures and vertebral rotations, segmentation using the integral spine model may face problems due to too large deviations from the normal spine. In this case, it is essential to select invariant features in order to capture a broad range of natural variations and simultaneously minimizing the effects of nonessential variations in ground-truth delineations. Also, it is important to carefully handle the alignment problem as this will be difficult, if not impossible, when dealing with much variation. A possible solution is to construct statistical spine models for different classes of abnormalities. This has already been proposed in [27]. However, as stated by Aykroyd and Mardia, even when different spine models are constructed for different spinal conditions, there would still be substantial variability within these conditions to obtain good statistical information. This remains an open problem.

A drawback of the reported method is the inherent difficulty of deformable models often getting trapped in local minima of optimization. It has been acknowledged previously that proper initialization is required to guarantee satisfying results in view of the presence of disturbing attractors in the image [32]. This is particularly true for complex images such as of the spine. As automatic initialization of deformable models is still an open problem [33], we deal with these problem by minimal human-computer interaction. The user simply points and clicks in the image to make one-to-one correspondence between model and image by means of six point landmarks per vertebra. The use of point landmarks alleviates the problem of interaction in 3-D space [33] due to their zero-dimensional property. During segmentation the user controls the entire spine model as a marionette by interaction with a few point landmarks and propagation of landmark solutions to other parts of the spine.

We conclude that the deformable integral spine model is a viable solution for interactive segmentation of 3-D spinal images. Future work will concentrate on improving and validating the constituents of the spine model, i.e., the necklace and strings models, on a statistically large number of segmented training images.

Acknowledgment

The authors thank F. Gerritsen from the Easy Vision Advanced Development, Philips Medical Systems, Best (The Netherlands), for providing the spinal CT images and the Easy Vision workstation. They are also thankful to J. Neuerburg from the Academic Hospital of the Heinrich-Heine University (Germany) and D. Bosch from the Academic Hospital of the Free University of Amsterdam (The Netherlands) for ground-truth segmentation.

References

[1] L. R. Long and G. R. Thoma, "Landmarking and feature localization in spine x-rays," *J. Electron. Imag.*, vol. 4, no. 10, pp. 939–956, 2001.

[2] S. Ghebreab and A. W. M. Smeulders, "Strings: Variational deformable models of multivariate ordered features," *IEEE Trans. Pattern Anal. Machine Intell.*, vol. 25, pp. 1399–1410, Nov. 2003.

[3] S. Ghebreab, P. R. Pfluger, and A. W. M. Smeulders, "Necklaces: Inhomogeneous and point-enhanced deformable models," *Computer Vision and Image Understanding*, pp. 96–117, 2002.

[4] C. Kauffmann and J. A. de Guise, "Digital radiography segmentation of scoliotic vertebral body using deformable models," *Proc. SPIE Medical Imaging*, vol. 3034, pp. 243–251, 1997.

[5] B. Verdonck, R. Nijlunsing, F. A. Gerritsen, J. Cheung, D. J. Wever, A. Veldhuizen, S. Devillers, and S. Makram-Ebeid, "Computer assisted quantitative analysis of deformities of the human spine," in *Lecture Notes in Computer Science*, W. H. Wells, A. Colchester, and S. Delp, Eds: Springer, 1998, Proc. Int. Conf. Medical Image Computing and Computer-Assisted Intervention, pp. 822–831.

[6] S. Benameur, M. Mignotte, S. Parent, H. Labelle, W. Skalli, and J. De Guise, "3D/2D registration and segmentation of scoliotic vertebrae using statistical models," *Computerized Med. Imag. Graphics*, vol. 27, no. 5, pp. 321–327, 2003.

[7] C. E. Aubin, J. Dansereau, Y. Petit, F. Parent, J. A. de Guise, and H. Labelle, "Three-dimensional measurement of wedged scoliotic vertebrae and intervertebral disks," *Eur. Spine J.*, vol. 7, no. 1, pp. 59–65, 1998.
[8] "Shape-Based Interactive Three-Dimensional Medical Image Segmentation," *Proc. SPIE Medical Imaging: Image Processing*, vol. 3034, pp. 236–242, 1997.
[9] K. P. Hinshaw, R. B. Altman, and J. F. Brinkley, "Shape-Based Models for Interactive Segmentation of Medical Images," *Proc. SPIE Medical Imaging 1995*, vol. 2434, pp. 771–780, 1995.
[10] R. Pichumani, H. Jadvar, A. M. Norbash, J. C. Drace, M. Tovar, and W. Murray, "Model-based finite-element three-dimensional segmentation and visualization of cervical spine ct images," in *Proc. RSNA 83rd Scientific Assembly Annu. Meeting*, Chicago, IL, 1997, pp. 118–118.
[11] R. Pichumani, "Construction of a three-dimensional geometric model for segmentation and visualization of cervical spine images," Ph.D. thesis, Stanford Univ., Stanford, CA, 1997.
[12] J. Bredno, T. M. Lehmann, and K. Spitzer, "A general discrete contour model in two, three, and four dimensions for topology-adaptive multichannel segmentation," *IEEE Trans. Pattern Anal. Machine Intell.*, vol. 25, pp. 550–563, May 2003.
[13] C. Lorenz and N. Krahnstöver, "Generation of point-based three-dimensional statistical shape models for anatomical objects," *Comput. Vis. Image Understanding*, vol. 77, no. 2, pp. 175–191, Feb. 2000.
[14] C. Lorenz and N. Krahnstoever, "3D statistical shape models for medical image segmentation," in *Proc. 2nd Int. Conf. 3-D Digital Imaging and Modeling, 1999*, 1999, pp. 4–8.
[15] T. Vrtovec, D. Tomazevic, B. Likar, and F. Pernus *et al.*, "Statistical shape deformable model of a lumbar vertebra," in *Proc. 8th Computer Vision Winter Workshop: Computer Vision—CVWW'03*, O. Drohlav *et al.*, Eds., Valtice, Czech Republic, 2003, pp. 91–96.
[16] I. Cohen, L. D. Cohen, and N. J. Ayache, "Using deformable surfaces to segment 3-D images and infer differential structures," in *Proc. Eur. Conf. Computer Vision*, 1992, pp. 648–652.
[17] L. H. Staib and J. S. Duncan, "Model-based deformable surface finding for medical images," *IEEE Trans. Med. Imag.*, vol. 15, pp. 720–731, Oct. 1996.
[18] T. McInerney and D. Terzopoulos, "Deformable models in medical image analysis: A survey," *Med. Image Anal.*, vol. 1, no. 2, pp. 91–108, Feb. 1996.
[19] M. Kass, A. P. Witkin, and D. Terzopoulos, "Snakes: Active contour models," in *Proc. IEEE Int. Conf. Computer Vision*, 1987, pp. 259–268.
[20] L. H. Staib and J. S. Duncan, "Boundary finding with parametrically deformable models," *IEEE Trans. Pattern Anal. Machine Intell.*, vol. 14, pp. 1061–1075, Nov. 1992.
[21] L. Piegl and W. Tiller, *The NURBS Book*, Berlin: Springer-Verlag, 1997.
[22] L. Haglund, "Adaptive multi-dimensional filtering," Ph.D. thesis, Linköping Univ., Linköping, Sweden, 1992.
[23] P. J. Besl and R. C. Jain, "Invariant surface characteristics for 3D object recognition in range images," *Comput. Vis. Graphics Image Processing*, vol. 33, no. 1, pp. 33–80, 1986.
[24] T. F. Cootes, G. J. Edwards, and C. J. Taylor, "Active appearance models," *IEEE Trans. Pattern Anal. Machine Intell.*, vol. 23, pp. 681–685, June 2001.
[25] N. Duta, A. K. Jain, and M. P. Dubuisson-Jolly, "Automatic construction of 2d shape models," *IEEE Trans. Pattern Anal. Machine Intell.*, vol. 23, pp. 433–446, May 2001.
[26] A. Neumann and C. Lorenze, "Statistical shape model based segmentation of medical images," *Computerized Med. Imag. Graphics*, vol. 22, pp. 133–143, 1998.
[27] R. G. Aykroyd and K. V. Mardia, "Shape Analysis of Spinal Curves by Wavelet Warping Using an MCMC Approach," Univ. Leeds, Leeds, U.K., Tech. Rep. STAT-96/10, 1996.
[28] G. Q. Wei, J. Z. Qian, and H. Schramm, "Generalized dynamic programming approaches for object detection: Detecting spine boundaries and vertebra endplates," in *Proc. IEEE Computer Vision Patern Recognition*, 2001, pp. 954–959.
[29] J. Ramsay and B. W. Silverman, *Functional Data Analysis*, Berlin, Germany: Springer-Verlag, 1997.
[30] B. S. Duran and P. K. Odell, *Cluster Analysis—A Survey*, Berlin, Germany: Springer-Verlag, 1974.
[31] S. Benameur, M. Mignotte, S. Parent, H. Labelle, W. Skalli, and J. De Guise, "Three-dimensional biplanar reconstruction of scoliotic vertebrae using statistical models," in *Proc. IEEE Int. Conf. Computer Vision and Pattern Recognition*, 2001, pp. 577–582.
[32] W. Neuenschwander, P. Fua, G. Szekely, and O. Kubler, "Initializing snakes," in *Proc. IEEE Conf. Computer Vision Patern Recognition*, 1994, pp. 658–663.
[33] A. F. Frangi, W. J. Niessen, R. M. Hoogeveen, van W. Walsum, and M. A. M. A. Viergever, "Model-based quantitation of three-dimensional magnetic resonance angiographic images," *IEEE Trans. Med. Imag.*, vol. 18, pp. 946–956, Oct. 1999.

Sennay Ghebreab received the M.Sc. and Ph.D. degrees from the University of Amsterdam, Amsterdam, The Netherlands, in 1996 and 2002 respectively. From 1996 to 2002 he was a Ph.D. degree student at the ISIS research group, Faculty of Sciences, University of Amsterdam, where he did research in the fields of visual learning from examples, model based analysis of images, and image retrieval by content.

He is co-organizer of the first international VISIM Workshop on Information Retrieval and Exploration in Large Medical Image Collections. Since 2002, he has been with the BIGR research group, Departments of Medical Informatics and Radiology, Erasmus MC, University Medical Center Rotterdam, The Netherlands. His current research focuses on the fundamentals of data analysis, information retrieval, and knowledge discovery in biomedical multimedia databases.

Arnold W. M. Smeulders (S'80–M'80) received the M.Sc. degree in physics from the Technical University of Delft, Delft, The Netherlands and the Ph.D. degree on the topic of visual pattern analysis from Leyden University in medicine, Leyden, The Netherlands, in 1982.

He heads the ISIS research group with research on theory, practice, and implementation of multimedia information analysis including image databases and computer vision and with an extensive record in co-operations with Dutch industry in the area of multimedia and video analysis. His current personal interest is characterized by semantic image retrieval, invariant representation of color and texture, the relation between pictures and language, learning vision, and the design of vision algorithms from first principles.HE received a Fulbright grant to spend at Yale University, New Haven, CT, in 1987, and a visiting professorship at the City University Hong Kong, Hong Kong, in 1996, and at ETL Tsukuba Japan in 1998.

In 2000, Dr. Smeulders was elected fellow of International Association of Pattern Recognition. He was an associate editor of IEEE TRANSACTIONS ON PATTERN ANALYSIS AND MACHINE INTELLIGENCE from 1996–2001. He is an honorary member of the Dutch Society for Pattern Recognition and director of the MultimediaN National initiative.